



LABORATÓRIO NACIONAL  
DE ENGENHARIA CIVIL

DEPARTAMENTO DE MATERIAIS  
Núcleo de Materiais Pétreos e Cerâmicos  
Núcleo de Materiais Metálicos

Proc. 0205/11/17684  
Proc. 0204/11/17692

# PHYSICAL-CHEMICAL CHARACTERIZATION OF HISTORIC PORTUGUESE TILES

Plano de Investigação Programada do LNEC

Lisboa • Janeiro de 2011

**I&D** MATERIAIS

RELATÓRIO 23/2011 – NPC/NMM



# PHYSICAL-CHEMICAL CHARACTERIZATION OF HISTORIC PORTUGUESE TILES

## ABSTRACT

A group of Portuguese tiles (azulejos) from the 17<sup>th</sup> to the early 19<sup>th</sup> centuries have been assessed for their chemical and mineralogical compositions and physical properties.

This LNEC Research Report includes the results of the characterization campaign that included chemical and mineralogical characterization of the glaze and ceramic bodies through x-ray fluorescence (XRF), x-ray diffraction (XRD) and thermogravimetric and differential thermal analysis (TGA-DTA). The pore structure and hydric behaviour of the azulejos have been studied through mercury intrusion porosimetry (MIP), BET specific surface measurements, water imbibition tests and hydrostatic weighing. The thermal and moisture expansion behaviours have also been assessed through dilatometric measurements.

Following the present results a data base was started where all similar data will be collected in the future to support consistently future research in the field.

# **CARACTERIZAÇÃO FÍSICO-QUÍMICA E MINERALÓGICA DE UM CONJUNTO DE AZULEJOS HISTÓRICOS PORTUGUESES DOS SÉCULOS XVII A XIX**

## **RESUMO**

Um grupo de azulejos portugueses dos séculos XVII a XIX foi caracterizado quanto à composição químico-mineralógica e propriedades físicas.

Este Relatório do LNEC inclui os resultados da campanha experimental que incluiu a caracterização química e mineralógica do vidro e corpo cerâmico dos azulejos através das técnicas de fluorescência de raios X (FRX), difracção de raios X (DRX) e análises termogravimétrica e térmica diferencial. A estrutura porosa e o comportamento hídrico dos azulejos foram estudados através de porosimetria de intrusão de mercúrio, análise da superfície específica pelo método de adsorção de azoto - BET, testes de imbibição de água e de pesagem hidrostática. Os comportamentos de expansibilidade térmica e hídrica foram estudados através de medições dilatométricas.

Utilizando os resultados deste relatório foi iniciada a construção de uma base de dados onde os resultados analíticos similares serão reunidos de forma consistente de maneira a poderem ser utilizados em projectos de investigação futuros na área dos azulejos históricos.

# PHYSICAL-CHEMICAL CHARACTERIZATION OF HISTORIC PORTUGUESE TILES

## INDEX

ABSTRACT.....	i
RESUMO .....	ii
1- INTRODUCTION .....	1
1.1 – Azulejos production process and resulting composition .....	3
2- MATERIALS AND METHODS .....	6
2.1- Azulejo samples .....	6
2.2- XRF analysis .....	7
2.3- DRX analysis.....	7
2.4- Thermogravimetric and differential thermal analysis (TGA-DTA) measurements.....	8
2.5- Water absorption coefficient and imbibition capacity.....	8
2.6- Hydrostatic weighing .....	8
2.7- Mercury intrusion porosimetry (MIP) .....	9
2.8- Surface area by nitrogen adsorption (BET).....	9
2.9- Moisture dilation .....	9
2.10- Thermal expansion coefficient.....	10
3- RESULTS AND DISCUSSION .....	11
3.1- Macroscopic and microscopic observations .....	11
3.2- Chemical and mineralogical characterization .....	13
3.2.1- Ceramic body composition by XRF.....	13
3.2.2- Ceramic body composition by XRD .....	16
3.2.3- Ceramic body TGA-DTA analysis .....	17
3.2.4- Glaze composition by XRF .....	18
3.3- Physical characterization and hydric behaviour .....	20
3.3.1- Open porosity and maximum water uptake .....	21
3.3.2- Mercury intrusion porosimetry analysis.....	21
3.3.3- BET Surface area .....	23

3.3.4- Capillary water absorption coefficient and water imbibition capacity	23
3.3.5- Moisture expansibility	25
3.3.6- Thermal expansibility	26
4- CONCLUSIONS	28
BIBLIOGRAPHIC REFERENCES	29
APPENDIX A – XRF SPECTRA AND REFERENCE SAMPLES USED FOR AZULEJOS GLAZE AND BISCUIT ANALYSIS	33
APPENDIX B – XRD DIFRACTOGRAMS	35
APPENDIX C – TGA-DTA CURVES	37
APPENDIX D – SUB-SAMPLES USED FOR WATER IMBIBITIONS TESTS	38
APPENDIX E – SUB-SAMPLES USED FOR THE MOISTURE DILATION AND THERMAL EXPANSIBILITY TESTS	39

# PHYSICAL-CHEMICAL CHARACTERIZATION OF HISTORIC PORTUGUESE TILES

## FIGURES INDEX

Figure 1 – Azulejo samples studied .....	6
Figure 2 - Moisture expansibility measurement set-up.....	10
Figure 3 - Schematic view of the XRF composition of the biscuits.....	15
Figure 4 - Schematic representation of the chemical composition of the glazes.	20
Figure 5 - Pore size distribution curves of the samples obtained with MIP .....	22
Figure 6 - Capillary water absorption curves.....	24
Figure 7 - Samples water dilation with time .....	25
Figure 8 - Thermal expansion curves of the sample tiles.....	26
Figure 9 - XRF spectrum of SP1-A1 biscuit. ....	33
Figure 10 - XRF spectrum of SP1-A1 glaze.....	33
Figure 11 – Diffractograms of the azulejos studied.....	36
Figure 12 - TGA and DTA curves of the analyzed samples. ....	37
Figure 13 – Sub-samples from the azulejo tiles studied during water imbibitions tests .....	38
Figure 14 - Azulejo sub-samples used for the moisture and thermal expansion tests.....	39

# PHYSICAL-CHEMICAL CHARACTERIZATION OF HISTORIC PORTUGUESE TILES

## TABLES INDEX

Table 1 - Ceramic biscuit macroscopic observations. ....	11
Table 2 - Macroscopic characteristics of the glaze of the samples studied.....	12
Table 3 - XRF results for the elemental composition of the ceramic bodies interpreted as oxides (weight %, normalized to 100%) .....	14
Table 4 - XRD results of the mineralogical composition of the ceramic bodies...	16
Table 5 – Weight percentage of calcite present in the ceramic body of tiles.....	17
Table 6 - XRF results of the elemental composition of the glazes .....	19
Table 7 - Hydrostatic weighing and vacuum saturation measurements. ....	21
Table 8 - Mercury intrusion porosimetry results. ....	22
Table 9 – Specific surface area of the ceramic biscuits .....	23
Table 10 - Capillary water absorption coefficient .....	24
Table 11 – Readings and values of water expansibility at 48 h .....	26
Table 12 - Thermal expansibilities of the sample tiles.....	27
Table 13 - Standards used for Glaze and biscuit quantification and indicative accuracy measurements (%) .....	34



# PHYSICAL-CHEMICAL CHARACTERIZATION OF HISTORIC PORTUGUESE TILES

## 1- INTRODUCTION

Architectural glazed ceramics – *azulejos* – are an important part of the cultural heritage of Portugal. But a sizeable part of this rich heritage is lost every year through continuous decay and neglect which results in the loss of the glaze layer that contains the decoration and in the desegregation of the ceramic body (the “biscuit”). This issue is particularly felt for glazed ceramics in architectural usage since they are subjected to much harsher environmental conditions. The physical, chemical and mineralogical characterization of *azulejos* is essential for a better understanding of their decay forms and mechanisms and to support studies on the best conservation and restoration measures to apply in order to protect this national heritage. It can also give information about their production technology, raw materials used and possible geographical provenance. However, despite the fact that many art history studies about Portuguese *azulejos* exist, there are only a few physical, chemical and mineralogical studies published on them.

Sanjad *et al.* made chemical and mineralogical characterizations of a group of 19<sup>th</sup>-early 20<sup>th</sup> century Portuguese tiles used in Belém do Pará in Brasil, contributing towards a better understanding of their constituent materials [1]. F. Antunes *et al* and Coroado *et at* have made some physical and mineralogical characterisations of a small group of Portuguese tiles from the 17<sup>th</sup> century [2, 3]. A. P. Carvalho made characterization studies of the ceramic pastes of historic tiles [4]. Other authors have performed studies in the characterisation of the glaze and pigments used in *azulejos* [5], including a Master Thesis by S. Coentro prepared at Laboratório Nacional de Engenharia Civil (LNEC) focusing on the

study of 17<sup>th</sup> century tiles glaze and pigments [6]. Despite the fact that such partial studies have been done on the physical, chemical and mineralogical characterization of azulejos glaze and biscuit materials there is not a comprehensive study on the matter.

Research needs on decay and how to deal with it have been pointed by J-M. Mimoso *et al.* in 2009 [7]. Such research must be based on a sound knowledge of the physical and chemical nature of azulejos and that need has been asserted in the research planning on the subject proposed also in 2009 by our group for internal financing. The approval of that plan lead to inspections to sites [8], research on decay [9] and a characterization campaign that included the previous study by S. Coentro [6] and now a more comprehensive study of which the first results are presented in this Report. The whole makes up a base of knowledge on historic Portuguese tiles that will allow a better understanding of their material properties, their influence on decay forms and mechanisms and hopefully a grounded effort on methods and materials for their conservation.

The main goal of the present study is to provide a detailed physical-chemical and mineralogical characterization of a group of ceramic tiles that present defects in their glaze layer. A further aim to be developed in future work at LNEC is to try and obtain correlations between the physical-chemical and mineralogical properties of the set of tiles studied in this report and their degradation mechanisms through the crystallization of soluble salts during accelerated ageing tests. Another aim is to survey the characterization techniques available that may be used by LNEC with a view to establish a preliminary database of the properties of historical Portuguese tiles that will be made available to all researchers working in the field.

The physical properties that have been studied presently were: i) the pore structure of the tiles ceramic body through mercury intrusion porosimetry (MIP); ii) the specific surface area through the BET method; iii) the water absorption curves; and iv) the thermal and moisture expansibility by dilatometric

measurements. The chemical and mineralogical constituents have been determined by x-ray fluorescence (XRF) of both the ceramic body and the glaze and x-ray diffractometry (XRD) of the ceramic body.

### **1.1 – Azulejos production process and resulting composition**

Ceramic tiles have generally a square shape and are considered a composite material made up of a ceramic body and a thin glass layer where the decorative pigments are integrated.

The raw clay materials used to prepare the ceramic biscuits were generally constituted by a mixture of crystalline minerals of diverse grain sizes such as clays, quartz, and feldspars. Calcite and dolomite could also be present on the raw materials or purposely added to them in order to promote the fusibility upon firing and to lighten the color of the final ceramic body. Other compounds such as organic matter, iron oxides, titanium oxide, pyrite, etc. could also be found in the raw materials in the form of impurities [10]. After the preparation of the ceramic paste and the molding of the biscuit, the raw ceramic bodies were fired in a traditional wood fuelled kiln. The use of such kilns made it difficult to control the firing procedure leading to inhomogeneous heating inside the oven, uncontrolled oxygenation and a range of firing temperatures that could range from around 800°C to circa 1100°C.

When fired in an oxidizing atmosphere the ceramic raw materials would react according to their initial composition, granulometry and firing temperature. At around 450-550°C the clay mineral structures dehydroxilate collapsing into illite - like structures [11]. Alkaline-earth silicates such as wollastonite and diopsides, earth-alkali aluminosilicates (such as gehlenite and anorthite); aluminosilicates (such as mullite), and other silicates such as cristobalite are formed together with fused vitreous phases [10]. At about 750°C calcium carbonate starts decomposing into calcium oxide. The smaller the grains of calcium carbonate the

faster and most complete will the transformation be [12]. The resulting calcium oxide reacts at carbonate-silicate interfaces with the clay minerals decomposition products to produce calcium aluminosilicates such as gehlenite and/or calcium magnesium aluminosilicates such as diopsides when magnesium is present. If this reaction is not complete residual calcium oxide may remain on the azulejos, this could re-hydrate and later re-carbonate originating a volume increase that may cause damage to the ceramic tiles structure, delayed distortion and crazing [12].

If the firing temperature is too low, un-reacted feldspars may remain, together with metakaolinite and un-bonded calcium or magnesium oxides [10]. After being fired, the ceramic body is composed of a highly heterogeneous matrix of crystal minerals and vitreous phases. The ratio of vitreous to amorphous phases depends on the raw materials and the firing temperatures, the vitreous phase increasing with the maximum temperature [10].

The glaze layer is thought to have been applied to the fired ceramic base by several procedures described elsewhere [10]. The glaze can be applied as a frit, as raw glaze materials or as a mixture of both. The final glaze is composed by an amorphous matrix with some crystalline inclusions such as quartz and chamotte (powdered ceramic biscuit). The vitreous matrix is composed mainly of a silica and lead oxide network with some alumina. Silica makes up the main vitreous network and lead oxide and alkaline oxides work as major fusing agents and network stabilizers. The use of lead oxide provides a suitable viscosity and elasticity during the firing procedure and produces a smooth and shiny glaze surface. Aluminum oxide is added to the glaze to stabilize and increase the chemical and physical resistance of the glaze structure, increase viscosity and to decrease the lead solubility. Calcium oxide acts as a network modifier. Historic Portuguese tiles are constituted by a lead-based glaze with minor amounts of sodium and potassium oxides and tin oxide as opacifying agent.

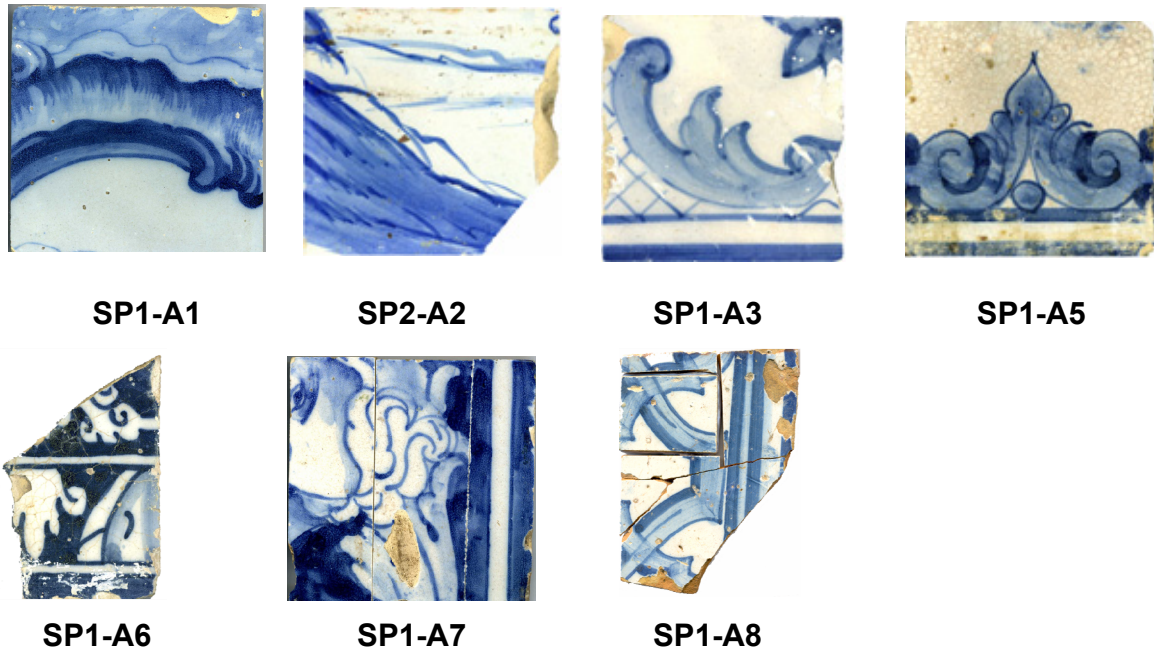
The common method of tiles production involves the initial firing of the clay body, as described, and the subsequent firing of the glaze. During the firing of the glaze a bonding is originated by the connection of the glaze to the ceramic body with integration between the materials in contact. The interface thus formed is highly important for establishing a good connection of the glaze to the ceramic body and may be determinant for better resistance to the decay factors that affect azulejos, particular the shear stresses that tend to delaminate the glaze from the biscuit [13].

The susceptibility of the azulejos towards decay depends on production parameters such as the raw clay and glaze compositions, the additions used, the moulding method, and the firing cycles. It also depends on the environmental exposure (particularly moisture), maintenance and contaminations that it may have withstood during its lifespan.

## 2- MATERIALS AND METHODS

### 2.1- Azulejo samples

Figure 1 shows the azulejo samples studied.



**Figure 1 – Azulejo samples studied**

Samples were tentatively dated taking in consideration their stylistic and technical features as follows:

- SP1-A1..... 18th century
- SP1-A2..... late 17th - early 18th century
- SP1-A3..... late 18th – early 19th century
- SP1-A5..... late 18th – early 19th century
- SP1-A6..... 17th century
- SP1-A7..... late 17th - early 18th century
- SP1-A8..... late 18th - early 19th century

## 2.2- XRF analysis

The samples were analysed by XRF at Universidade Nova de Lisboa (UNL) within a research partnership between LNEC and UNL. The analysis were performed directly on an ArtTAX Pro spectrometer manufactured by Intax GmbH and equipped with a Molybdenum X- ray source of about 70  $\mu\text{m}$  diameter and a siliceous detector X-Flash. This equipment allowed sample analysis of elements between aluminium (Al) and uranium (U).

For the glaze analysis direct measurements were performed on the white surface areas of the tiles. For the analysis of the ceramic biscuit, the samples were powdered to a grain size  $<106 \mu\text{m}$  and used simultaneously for XRF and DRX analyses. The powdered samples were put on top of a glass slide and compacted with a spatula into a layer or about 3 mm thickness. Three measurements were taken at distinct spots of the samples in a helium atmosphere with an acquisition time of 300s at 40 kV and 600  $\mu\text{A}$  excitation source intensity.

The quantitative analysis of the spectra was performed with the *WinAxil and Winfund programs* using the fundamental parameters method. A lead glass reference (CMOG C) and a lead and tin glass standard prepared by UNL (LeadTin) were used for the calibration of the glazes. A red brick clay standard (Red Brick Clay 679) and a Plastic clay standard (Plastic clay 98b) were used for the calibration of the ceramic biscuit measurements. The standards composition is presented in Appendix A.

The accuracy of the method has been determined through the analysis of the (CMOG C) standard for the glaze and plastic clay standard for the ceramic biscuits (Appendix A).

## 2.3- DRX analysis

A part of the ceramic body was removed from the tile, separated from the glaze layer with a saw and carefully cleaned of any remaining mortar. The ceramic body samples were then dried at 60°C up to constant weight, and crushed until all particles passed a 106  $\mu\text{m}$  sieve. A total of 2 g per sample has been analysed

on a Philips X-Pert X-ray diffractometer with cobalt K $\alpha$  radiation. The analysis conditions used were: screening between 3 and 74° 2 $\theta$ , 0.05°2 $\theta$  /s; 35 kV and 45 mA.

#### 2.4- Thermogravimetric and differential thermal analysis (TGA-DTA) measurements

The powdered samples (<106  $\mu$ m) were dried at 60°C and analysed in a Setaram TGA 92 thermal analysis equipment (TGA-DTA) in an argon atmosphere (3L/h). The heating rate was 10°C/min from room temperature to 1000°C.

#### 2.5- Water absorption coefficient and imbibition capacity

The samples have been isolated laterally with Sikadur 32N epoxy resin and dried at 60°C up to constant weight. The samples were then positioned flat over a container with demineralised water. The water wetted about 0.5 cm of the tile height. The water absorption increment was monitored by periodic weighing of the samples.

#### 2.6- Hydrostatic weighing

The experimental was made according to a LNEC procedure [14] based on the EN-1936 European Standard. The tile samples are dried up to constant weight at 60°C. Their dry weight (M1) is noted. They are then put in a vacuum chamber and let to degasify for 24 h, after which demineralised water is introduced until the samples are covered and then again let in a vacuum for another 24 h. The atmospheric pressure is then re-established and the samples are left immersed in water for another 24 h. Their weights while immersed in water (M2) and removed but still wet (M3) are taken. The values for open porosity (P), maximal water uptake (MWU), real (DR) and apparent densities (AD) are then obtained through the following equations:

$$DR = (M1 - M2) \quad (Kg.m^{-3}) \quad \text{Eq. 1}$$

$$AD = \left( \frac{M1}{M3 - M2} \right) \quad (Kg.m^{-3}) \quad \text{Eq. 2}$$



$$P = \left( \frac{M3 - M1}{M3 - M2} \right) (\%) \quad \text{Eq. 3}$$

$$MWU = \left( \frac{M3 - M1}{M1} \right) (\%) \quad \text{Eq. 4}$$

### 2.7- Mercury intrusion porosimetry (MIP)

Before the MIP analysis the samples are dried up to constant weight at 60°C in a ventilated oven, cooled down in an exsicator and weighed with an analytical scale. The MIP measurements have been performed with a Quantachrome Autoscan porosimeter at LNEC according to an LNEC procedure LERO-PE15 [15], based on the ASTM D4404-84 American Standard.

### 2.8- Surface area by nitrogen adsorption (BET)

The samples are dried up to constant weight at 60°C in a ventilated oven, cooled down in an exsicator and weighed in an analytical scale. The surface area determination by the BET theory has been measured with Quantachrome AutoSorb1 equipment, according to LNEC E412 Specification [16].

### 2.9- Moisture dilation

The moisture expansion has been measured using Linear Strain Conversion (LSC) transducers Full Bridge 350 according to LNEC procedure LERO PE-10 [17] based on the RILEM 25 PEM Provisional Recommendations.

The samples were cut in lengths from 50 to 85 mm. On the top was glued a glass slice with a small incision to allow the transducer point to rest and avoid any slippage or penetration into the ceramic body. The samples are dried at 60°C in a ventilated oven and allowed to cool down in an exsicator before the measurement procedure. Each sample and transducer were mounted on a stainless steel structure, put inside a cylindrical acrylic container and covered with deionised water (see Figure 2). The tests were performed at laboratory conditions (20 ± 2°C). The lengths were registered every 5 min up to 48 h.

The linear coefficient of hydric dilation ( $\epsilon$ ) is calculated after 48 h of immersion through the formula:

$$\varepsilon = \left( \frac{L_f - L_0}{l_0} \right)$$

**Eq. 5**

where  $L_f$  is the transducer reading at 48 h;  $L_0$  the initial transducer reading; and  $l_0$  the initial sample length.



Figure 2 - Moisture expansibility measurement set-up.

### 2.10- Thermal expansion coefficient

The thermal expansibility is measured with an automatic dilatometer Dilatomic 1200C manufactured by Theta Industries, with 1  $\mu\text{m}$  resolution on the length measurement and 0.1 $^{\circ}\text{C}$  on the surface temperature of the sample. The experimental procedure was performed according to the EN-14581 Standard [18].








The temperature program initiated at around 20 $^{\circ}\text{C}$  with temperature increments of 20 $^{\circ}\text{C}$ , a stabilization period of 120 min at each temperature step up to a temperature of 120 $^{\circ}\text{C}$ . The thermal expansion coefficients ( $\xi$ ) were calculated by regression from the  $\Delta L / L$  values obtained at the end of each temperature step, where  $L$  is the initial sample length and  $\Delta L$  is the length variation measured at the end of each step.

### 3- RESULTS AND DISCUSSION

#### 3.1- Macroscopic and microscopic observations

The ceramic body is generally characterized by a light yellow-cream to pink-oranje colour, fine texture, sometimes with long pores oriented parallel to the surface and dispersed in the matrix (Table 1).

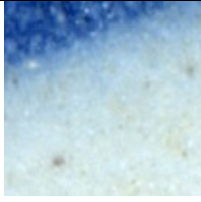

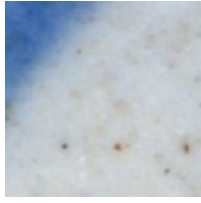

Table 1 - Ceramic biscuit macroscopic observations.

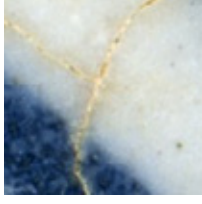
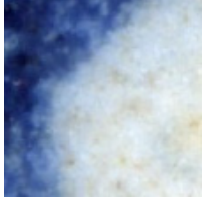
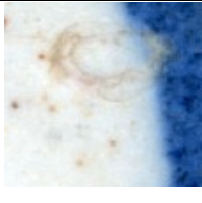
<b>Samples</b>	<b>Picture</b>	<b>thickness</b>	<b>Observations</b>
<b>SP1-A1</b>		11-12mm	Yellow colour with small circular and elongated pores.
<b>SP1-A2</b>		14mm	Yellow colour with small circular and elongated pores.
<b>SP1-A3</b>		11mm	Yellow-orange colour with small circular and elongated pores.
<b>SP1-A5</b>		11-12mm	Yellow colour with large and small elongated pores. Large air pockets resulting from the plastic conformation method of the ceramic paste used to shape the biscuit.
<b>SP1-A6</b>		15mm	Yellow colour with small circular and elongated pores. The ceramic matrix has a less consistent appearance.
<b>SP1-A7</b>		13mm	Yellow-orange colour with small circular and elongated pores.
<b>SP1-A8</b>		10mm	Main body pink with a yellowish sub-layer below the glaze. Elongated pores.

In some cases there are heterogeneities in the ceramic matrix, such as red inclusions several mm in length. These aspects indicate the use of a rather rough ceramic paste or mixture of clays. The presence of elongated pores is a consequence of the plastic conformation of the raw clay materials for shaping the tiles where the largest dimension of the pores is parallel to the tile surface. The layering of colours usually indicates a poor mixing of the clays used but in the case of sample SP1-A8 (see Table 1) it suggests the application of a lighter clay layer under the glaze in order to lighten the biscuit and avoid a dark shade under the partially transparent glaze.

In (Table 2) some macroscopic observations of the glaze layer of the samples are schematized.

Table 2 - Macroscopic characteristics of the glaze of the samples studied

		<b>Colours</b>	<b>Delamination</b>	<b>Other defects</b>
<b>SP1-A1</b>		Blue on lighter blue	No	Lack of glaze; Presence of pores
<b>SP1-A2</b>		White, Blue	No	Lack of glaze; Impact damage; Pores
<b>SP1-A3</b>		White, Blue	No	Lack of glaze; Crawling; Pores
<b>SP1-A5</b>		White, Blue	No	Craquelé; Pores; Presumed organic contamination

<b>SP1-A6</b>		White, Blue	Yes	Lack of glaze; Craquelé; Delamination ; Pores
<b>SP1-A7</b>		White, Blue	Yes	Pores; Delamination; Possible shivering Nicks on edges
<b>SP1-A8</b>		White, Blue	Yes	Impact damage; Pore; Circular blisters (?) in the glaze

### **3.2- Chemical and mineralogical characterization**

#### **3.2.1- Ceramic body composition by XRF**

The XRF chemical composition results (weight %) of the ceramic bodies are included in Table 3. The SiO<sub>2</sub> percent contents vary from 39 to 44 %, the CaO from 35 to 41 % and the Al<sub>2</sub>O<sub>3</sub> from 12-15 %. Lead has also been identified in all samples with a residual content of 200 - 900 ppm (less than 0.01%).

Table 3 - XRF results for the elemental composition of the ceramic bodies interpreted as oxides (weight %, normalized to 100%)

Oxides	Al <sub>2</sub> O <sub>3</sub>	CaO	Cr <sub>2</sub> O <sub>3</sub>	CuO	Fe <sub>2</sub> O <sub>3</sub>	K <sub>2</sub> O	MnO	NiO	PbO	SiO <sub>2</sub>	SrO	TiO <sub>2</sub>	ZnO
Samples	%	%	%	%	%	%	%	%	%	%	%	%	%
<b>SP1-A1</b>	<b>13.4</b>	<b>35.5</b>	<b>0.01</b>	<b>0.01</b>	<b>5.4</b>	<b>1.3</b>	<b>0.03</b>	<b>0.01</b>	<b>.0002</b>	<b>43.5</b>	<b>0.05</b>	<b>0.8</b>	<b>0.02</b>
<i>STD</i>	0.5	0.5	0.001	0.001	0.1	0.3	0.003	.002	.0001	1.3	.0002	0.2	.001
<b>SP1-A2</b>	<b>12.1</b>	<b>39.0</b>	<b>0.01</b>	<b>0.01</b>	<b>4.9</b>	<b>1.9</b>	<b>0.04</b>	<b>0.01</b>	<b>0.07</b>	<b>41.3</b>	<b>0.05</b>	<b>0.7</b>	<b>0.02</b>
<i>STD</i>	1.1	2.3	0.001	0.001	1.2	0.4	0.008	.001	0.003	3.9	0.004	0.1	.003
<b>SP1-A3</b>	<b>12.5</b>	<b>38.2</b>	<b>0.01</b>	<b>0.01</b>	<b>5.2</b>	<b>1.8</b>	<b>0.04</b>	<b>0.01</b>	<b>0.002</b>	<b>41.6</b>	<b>0.06</b>	<b>0.6</b>	<b>0.03</b>
<i>STD</i>	0.5	1.3	0.006	0.003	0.3	0.2	0.002	.002	.0004	1.6	.0004	0.06	0.5
<b>SP1-A5</b>	<b>14.6</b>	<b>36.4</b>	<b>0.01</b>	<b>0.01</b>	<b>5.4</b>	<b>1.6</b>	<b>0.04</b>	<b>0.01</b>	<b>0.05</b>	<b>41.0</b>	<b>0.05</b>	<b>0.8</b>	<b>0.02</b>
<i>STD</i>	0.8	0.5	0.001	.0001	0.4	0.3	0.005	.002	0.06	1.5	0.003	0.03	0.8
<b>SP1-A6</b>	<b>12.5</b>	<b>37.2</b>	<b>0.01</b>	<b>0.01</b>	<b>4.8</b>	<b>1.2</b>	<b>0.05</b>	<b>0.01</b>	<b>0.03</b>	<b>42.9</b>	<b>0.06</b>	<b>1.1</b>	<b>0.02</b>
<i>STD</i>	0.7	2.5	0.004	0.002	0.2	0.1	0.008	.001	0.06	2.7	0.001	0.52	0.7
<b>SP1-A7</b>	<b>12.1</b>	<b>41.3</b>	<b>0.01</b>	<b>0.02</b>	<b>5.1</b>	<b>1.5</b>	<b>0.05</b>	<b>0.01</b>	<b>0.002</b>	<b>39.0</b>	<b>0.06</b>	<b>0.9</b>	<b>0.02</b>
<i>STD</i>	1.0	1.3	0.001	0.004	0.4	0.1	0.004	.001	.0001	1.9	0.005	0.25	1.0
<b>SP1-A8</b>	<b>13.7</b>	<b>35.2</b>	<b>0.01</b>	<b>0.01</b>	<b>6.6</b>	<b>2.4</b>	<b>0.04</b>	<b>0.01</b>	<b>0.09</b>	<b>40.9</b>	<b>0.04</b>	<b>0.9</b>	<b>0.02</b>
<i>STD</i>	0.5	1.5	0.000	0.003	1.0	0.4	0.003	.003	0.003	0.9	0.002	0.16	0.5

The presence of lead in the ceramic biscuit could be explained by the absorption of the soluble lead oxide used in the glaze formulation, or because of leaching of soluble lead from the glaze. In order to be able to discriminate between the use of a raw glaze or frit, comparative studies should be performed on the contents of lead present in the ceramic body when each preparation method is used for the manufacture of azulejos (through reproductions). However, the low content in lead seems compatible with the use of previously prepared frits.

The body colour is generally related to the amount and distribution of Fe<sup>3+</sup> ions such as in Fe<sub>2</sub>O<sub>3</sub> present in the ceramic matrix. The samples usually presented a cream or light yellow-orange colour indicative of a low content of Fe<sub>2</sub>O<sub>3</sub>. Sample

SP1-A8 depicted the darkest shade of pink-orange (Table 1) which corresponds to the slightly higher amount of  $\text{Fe}_2\text{O}_3$  detected by XRF.

A schematic representation of the ceramic biscuit azulejos composition is presented in Figure 3.

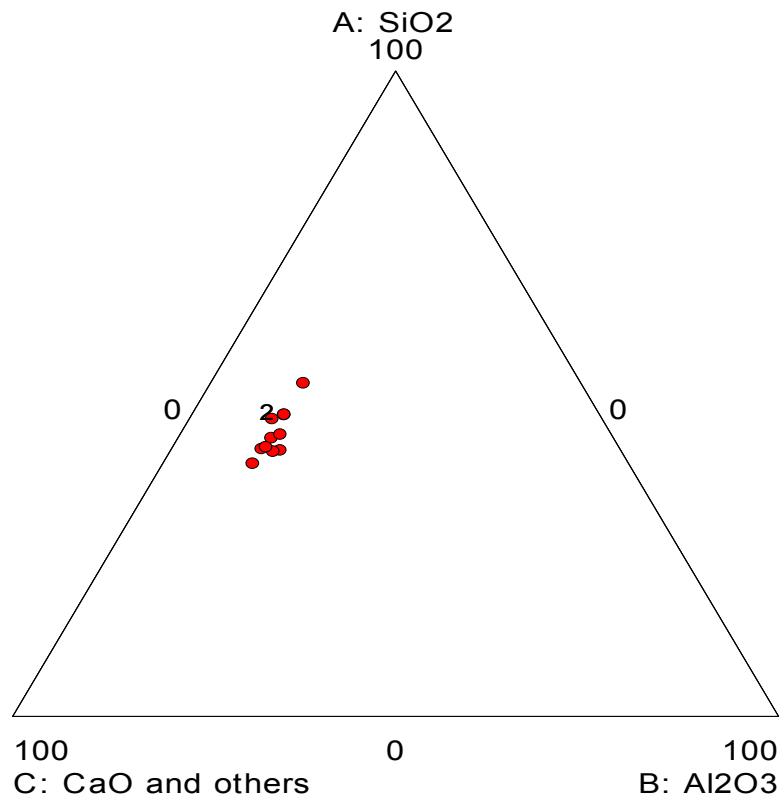


Figure 3 - Schematic view of the XRF composition of the biscuits

The results of the elemental composition may indicate that the raw materials used in the production of the ceramic pastes had similar compositions. The raw materials could be classified as high Ca-rich ( $\text{CaO} > 6\%$ ) and low refractory (fluxes such as  $\text{K}_2\text{O}$ ,  $\text{CaO}$ ,  $\text{TiO}_2 > 9\%$ ) clays [19]. The mineralogical composition (Table 4) is more distinct suggesting that the raw materials mineralogy, granulometry and/or firing conditions were considerably different.

### 3.2.2- Ceramic body composition by XRD

The minerals identified by XRD are presented in Table 4. The minerals identified in the set of tile samples are similar with different semi-quantitative amounts. The corresponding diffractograms can be found in Annex C.

Table 4 - XRD results of the mineralogical composition of the ceramic bodies

Mineral name	Quartz (Q)	Cristobalite (Cr)	Calcite (C)	Gehlenite (G)	Wollastonite (W)	K-Feldspars (F)	Hematite (H)	Analcime (A)
Chemical formula	SiO <sub>2</sub>	SiO <sub>2</sub>	CaCO <sub>3</sub>	Ca <sub>2</sub> Al[AlSiO <sub>7</sub> ]	CaSiO <sub>3</sub>	KAlSi <sub>3</sub> O <sub>8</sub>	Fe <sub>2</sub> O <sub>3</sub>	NaAlSi <sub>2</sub> O <sub>6</sub> ·H <sub>2</sub> O
Samples	Q	Cr	C	G	W	F	H	A
SP1-A1	++/+++	-	-	++	++/+++	+	+	Tr/+
SP1-A2	+ /++	Tr	++	++	+	+	Tr	Tr
SP1-A3	++/+++	-	+ /++	++	++	+	Tr/+	-
SP1-A5	+ /++	Tr	+	++	++	+	Tr/+	+
SP1-A6	++/+++	+	++	++/+++	Tr	++	Tr/+	+ /++
SP1-A7	++	-	++	++/+++	Tr/+	+	Tr/+	-
SP1-A8	++/+++	-	+ /++	++	++	+ /++	Tr/+	Tr

Semi-quantitative analysis of the minerals: +++ high, ++ medium, + low, "Tr" traces and "-" not detected

Quartz is generally used as main constituent of the body and glaze compositions, acts as filler and contributes to dimensional stability by reducing firing shrinkage [12]. Quartz was present in all samples and was one of the major minerals present together with wollastonite for SP1-A1 and gehlenite for SP1-A6 and SP1-A7. The other mineral phases encountered were cristobalite, calcite, hematite, feldspars and analcime. Gehlenite and wollastonite are reported to be formed at temperatures > 800°C [11] being present in all samples. Besides cristobalite, other minerals formed at high firing temperatures such as mullite (>900°C) [11], were not detected in the samples analysis.



Calcite is present in all samples and it was doubly confirmed through the TGA-DTA measurements (Table 5) but due to the low amount present in SP1-A1 its presence could not be identified via XRD. The calcite present can be the result of contamination from the mortars or due to re-hydration of the CaO formed during the firing and later re-carbonation into calcite.

### 3.2.3- Ceramic body TGA-DTA analysis

Thermal variations associated with the chemical and physical transformations, such as decomposition of carbonates ( $\text{CaCO}_3$ ) in the range 600-850°C, were obtained by TGA-DTA analysis. From these data, the amount of calcite was calculated (Table 5) and the results of XRD could be confirmed (Table 4). All decarbonation registered was assumed to be due to the decomposition of calcite since there was no information about the existence of other carbonates in the samples by XRD or XRF. The graphical results obtained are presented on Appendix C.

Table 5 – Weight percentage of calcite present in the ceramic body of tiles.

<b>Samples</b>	<b>Calcite (%)</b>
<b>SP1-A1</b>	1.0
<b>SP1-A2</b>	25.3
<b>SP1-A3</b>	11.7
<b>SP1-A5</b>	3.0
<b>SP1-A6</b>	18.6
<b>SP1-A7</b>	24.5
<b>SP1-A8</b>	12.0

The results show large variations on the calcite present in the samples but there is a group of high content (SP1-A2 and SP1-A7) and a group of very low content (SP-A1 and SP-A5).

The presence of calcite may have several origins: incomplete de-carbonation in the core of the ceramic tile during firing, re-carbonation of un-reacted calcium oxide and contamination with soluble CaO/CaCO<sub>2</sub> from the mortars [20, 21]. The presence of high level of carbonates in the raw ceramic materials promotes high porosity due to de-carbonation during firing, lowers the vitrification temperature (to 700-800°C) [22] and may produce lighter colored ceramic pastes.

#### 3.2.4- Glaze composition by XRF

The results of the compositional analysis of the glazes are included in Table 6 in the form of oxides. The content of SiO<sub>2</sub> measured varied from 52% to 71%. Due to *u*-XRF low sensitivity to Al determination and the small amounts present in the samples the quantification of Al<sub>2</sub>O<sub>3</sub> present, the other network forming oxide, could not be accurately measured. In relation to the network modification oxides the values of PbO vary from 15 to 31%; K<sub>2</sub>O from 5 to 9%; CaO from 0.6 to 1.1 % while Na<sub>2</sub>O could not be determined again due to XRF limitations. Opacifying or colouring oxides such as CuO and Fe<sub>2</sub>O<sub>3</sub> were found as minor components (<0.4%) while SnO<sub>2</sub> was found with a content of 5-11 %.

Table 6 - XRF results of the elemental composition of the glazes  
(Weight %, normalized to 100%)

Oxides	CaO	CuO	Fe <sub>2</sub> O <sub>3</sub>	K <sub>2</sub> O	MnO	NiO	PbO	SiO <sub>2</sub>	SnO <sub>2</sub>
Samples	%	%	%	%	%	%	%	%	%
<b>SP1-A1</b>	<b>0.8</b>	<b>0.1</b>	<b>0.1</b>	<b>6.3</b>	<b>0.01</b>	<b>0.04</b>	<b>19.6</b>	<b>62.7</b>	<b>10.3</b>
<i>STD</i>	<i>0.081</i>	<i>0.003</i>	<i>0.0211</i>	<i>0.3</i>	<i>0.0016</i>	<i>0.009</i>	<i>1.46</i>	<i>1.4</i>	<i>0.20</i>
<b>SP1-A2</b>	<b>0.7</b>	<b>0.02</b>	<b>0.3</b>	<b>6.1</b>	<b>0.01</b>	<b>0.02</b>	<b>24.7</b>	<b>63.5</b>	<b>4.7</b>
<i>STD</i>	<i>0.081</i>	<i>0.003</i>	<i>0.0211</i>	<i>0.3</i>	<i>0.0016</i>	<i>0.009</i>	<i>1.46</i>	<i>1.4</i>	<i>0.20</i>
<b>SP1-A3</b>	<b>0.6</b>	<b>0.02</b>	<b>0.3</b>	<b>7.2</b>	<b>0.01</b>	<b>0.06</b>	<b>24.9</b>	<b>60.3</b>	<b>6.7</b>
<i>STD</i>	<i>0.030</i>	<i>0.001</i>	<i>0.0109</i>	<i>0.2</i>	<i>0.0003</i>	<i>0.002</i>	<i>0.46</i>	<i>0.7</i>	<i>0.07</i>
<b>SP1-A5</b>	<b>0.6</b>	<b>0.02</b>	<b>0.3</b>	<b>7.2</b>	<b>0.01</b>	<b>0.03</b>	<b>19.7</b>	<b>68.0</b>	<b>4.2</b>
<i>STD</i>	<i>0.044</i>	<i>0.002</i>	<i>0.0237</i>	<i>0.3</i>	<i>0.0011</i>	<i>0.008</i>	<i>0.75</i>	<i>1.1</i>	<i>0.04</i>
<b>SP1-A6</b>	<b>1.1</b>	<b>0.01</b>	<b>0.4</b>	<b>8.5</b>	<b>0.01</b>	<b>0.07</b>	<b>14.8</b>	<b>70.5</b>	<b>4.6</b>
<i>STD</i>	<i>0.046</i>	<i>0.001</i>	<i>0.0527</i>	<i>0.2</i>	<i>0.0005</i>	<i>0.011</i>	<i>0.40</i>	<i>0.3</i>	<i>0.27</i>
<b>SP1-A7</b>	<b>0.9</b>	<b>0.03</b>	<b>0.4</b>	<b>6.4</b>	<b>0.02</b>	<b>0.02</b>	<b>24.9</b>	<b>58.0</b>	<b>9.3</b>
<i>STD</i>	<i>0.064</i>	<i>0.001</i>	<i>0.0250</i>	<i>0.2</i>	<i>0.0006</i>	<i>0.004</i>	<i>0.38</i>	<i>1.7</i>	<i>1.10</i>
<b>SP1-A8</b>	<b>0.8</b>	<b>0.02</b>	<b>0.2</b>	<b>5.4</b>	<b>0.01</b>	<b>0.03</b>	<b>31.1</b>	<b>51.8</b>	<b>10.7</b>
<i>STD</i>	<i>0.001</i>	<i>0.001</i>	<i>0.0002</i>	<i>0.1</i>	<i>-</i>	<i>0.000</i>	<i>0.03</i>	<i>0.2</i>	<i>0.01</i>

A schematic representation of the ceramic biscuit azulejos composition is presented in Figure 4.

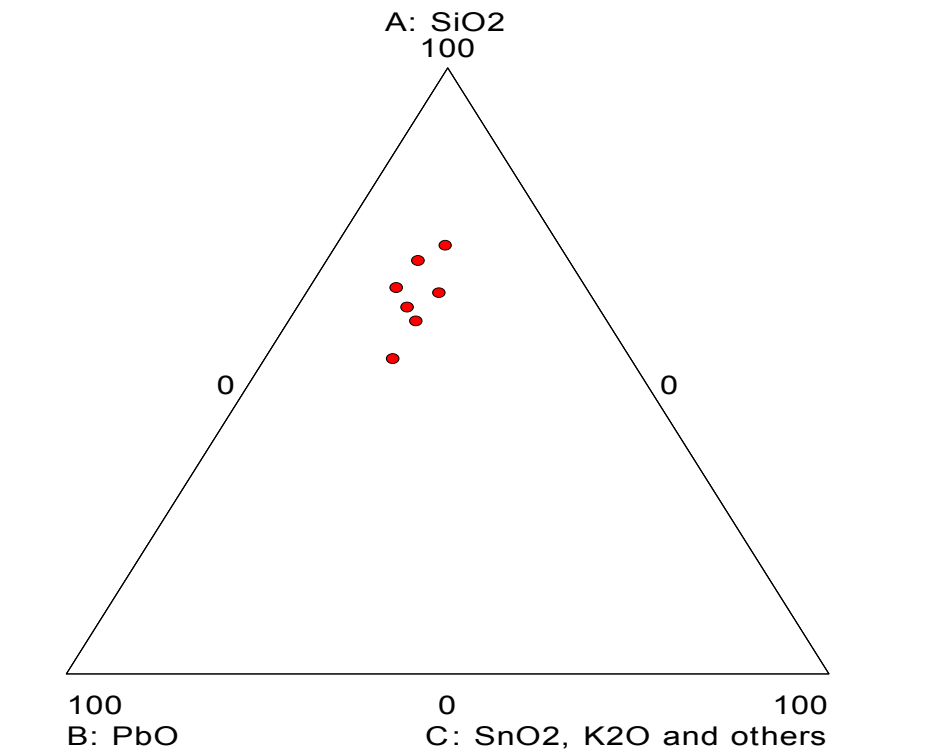


Figure 4 - Schematic representation of the chemical composition of the glazes

### **3.3- Physical characterization and hydric behaviour**

Physical characteristics of the samples such as porosity, density and water absorption capacity are directly related with the raw materials used, the morphologic and mineralogical transformations occurred in kiln atmosphere and the later degradation mechanisms of porous architectural ceramic materials.

The structure of the ceramic paste is composed of irregular unions between very thin grains to vitreous masses that connect larger and harder grains such as quartz, chamotte, etc [10]. These agglomerate masses are crossed by numerous thin pores, with micro-fissures and other cavities of different sizes filled with air usually resulting from the ceramic paste preparation methods. The pore structure of the ceramic paste is also a consequence of the loss of structural water from the clay minerals, the ( $\alpha$ - $\beta$ ) quartz transformation and consequent volumetric

expansion at 575°C and the release of CO<sub>2</sub> from the carbonate materials [10]. As the firing temperature increases, the vitrification also increases and the pore size decreases [10].

In architectural ceramics the pore volume and pore size determine the capacity of fluids storage and ease of fluid circulation within the materials.

### 3.3.1- Open porosity and maximum water uptake

Table 7 - Hydrostatic weighing and vacuum saturation measurements.

<b>Samples</b>	<b>Real density (kg/m<sup>3</sup>)</b>	<b>Apparent density (kg/m<sup>3</sup>)</b>	<b>Open porosity (vol %)</b>	<b>Maximum water uptake (mass %)</b>
<b>SP1-A1</b>	2870	1600	44.3	27.6
<b>SP1-A2</b>	2730	1730	36.6	21.1
<b>SP1-A3</b>	2820	1620	42.7	26.4
<b>SP1-A5</b>	2740	1620	40.9	25.3
<b>SP1-A6</b>	2750	1720	37.7	22.0
<b>SP1-A7</b>	2810	1710	39.0	22.8
<b>SP1-A8</b>	2790	1712	38.6	22.6

The densities of the samples tested are relatively similar with a higher open porosity for the SP1-A1 tile and lower for SPA-A2 and SP1-A6 tiles with a corresponding water uptake. Some differences exist in the porosity accessible to water with higher open porosity values for SP1-A1 and SP1-A3 tiles and lower values for SP1-A2 and SP1-A6 tiles.

### 3.3.2- Mercury intrusion porosimetry analysis

The porosity values obtained through mercury intrusion porosimetry (MIP) follow the general trend values obtained from the measurement of the water intake

(Table 7) except for SP1-A5. The difference obtained for this sample could be explained by the existence of large pores (see Table 1) which are beyond the measuring capability of the protocol used.

The pore size distribution of the samples are presented in Figure 5 and Table 8. Most samples present unimodal pore distributions in the region of 0.5 – 0.7  $\mu\text{m}$ . However SP1-A2, SP1-A7 and SP1-A8 present a bimodal pore size distribution where SP1-A8 presenting a high rate of small pores with diameters around 0.02-0.07  $\mu\text{m}$ .

Table 8 - Mercury intrusion porosimetry results.

Samples	Porosity (%)	Pores ( $\mu\text{m}$ )
SP1-A1	46.9	0.7
SP1-A2	34	0.04 - 0.46
SP1-A3	45.5	0.45
SP1-A5	31.7	0.7
SP1-A6	38.7	0.29 - 0.68
SP1-A7	33.3	0.03 – 0.45
SP1-A8	36.2	0.02 - 0.065

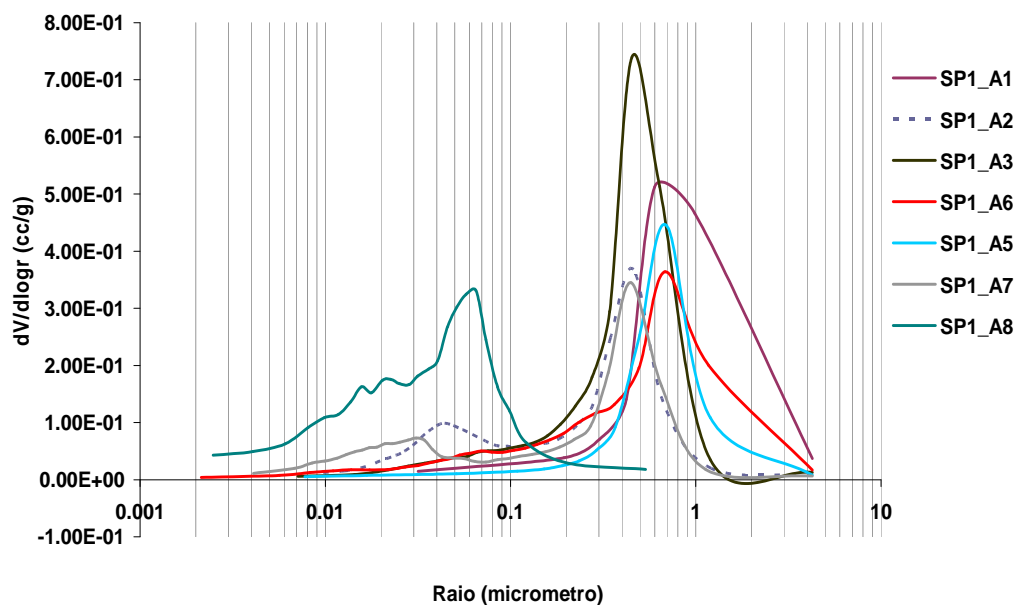


Figure 5 - Pore size distribution curves of the samples obtained with MIP

### 3.3.3- BET Surface area

Nitrogen adsorption analysis according to the BET theory was the reference method for specific surface area analysis. The results for the ceramic biscuits are presented in Table 9. Samples SP1-A7 and SP1-A8 could not be measured due to an equipment malfunction.

Table 9 – Specific surface area of the ceramic biscuits

<b>Samples</b>	<b>Spec. surf. area (m<sup>2</sup>/g)</b>
<b>SP1-A1</b>	3.77
<b>SP1-A2</b>	3.68
<b>SP1-A3</b>	1.69
<b>SP1-A5</b>	3.91
<b>SP1-A6</b>	1.63
<b>SP1-A7</b>	-
<b>SP1-A8</b>	-

### 3.3.4- Capillary water absorption coefficient and water imbibition capacity

The results seen on Figure 6 and Table 10 relate to the different capacities of fluids transfer of the tiles. The higher open porosity measured for SP1-A1 results in a much higher speed of water imbibition of this sample compared to the others. A correlation may in fact be established between the values of the open porosity determined through water intake and MIP and the water absorption coefficients presented in Table 7 and Table 8.

The capillary water absorption curves of SP1-A1 and SP1-A3, made up of two straight lines, are characteristic of materials whose pores are well interconnected and lay in a defined pore dimensional range as observed in Figure 6. The low imbibition capacity and small capillarity coefficient observed for sample SP1-A5 may be explained by the presence of organic contamination materials impregnated in the ceramic body and glaze of the sample that could act as water

repellent hydrophobic agents. That sample has in fact been collected from the oven area of an old kitchen.

The low water absorption coefficients of samples SP1-A8, SP1-A7 and SP1-A2 can be explained by the existence of pores with distinct sizes (bimodal pore size distribution, Figure 5).

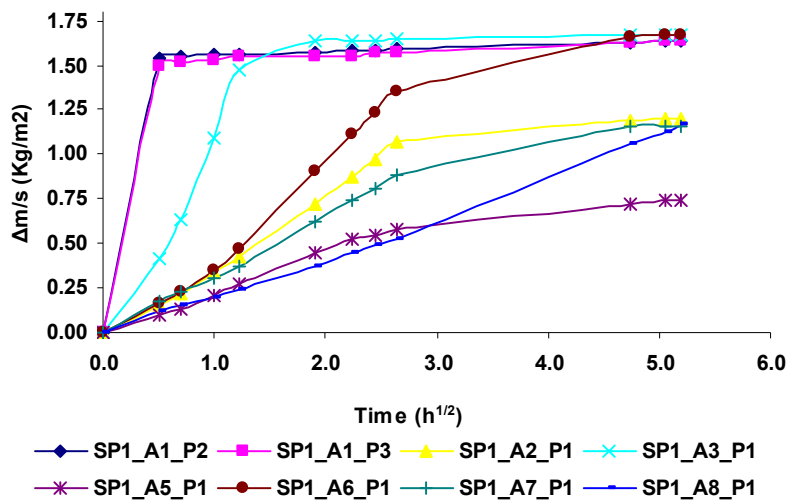


Figure 6 - Capillary water absorption curves.

Table 10 - Capillary water absorption coefficient

Samples	Cap. Coef. (Kg/m <sup>2</sup> /h <sup>1/2</sup> )	Imbibition capacity (% Wt)
SP1-A1-P2	3.1	16
SP1-A1-P3	3.0	15
SP1-A2-P1	0.4	12
SP1-A3-P1	1.2	17
SP1-A5-P1	0.2	7
SP1-A6-P1	0.5	17
SP1-A7-P1	0.3	12
SP1-A8-P1	0.2	12



Note: the additional codes “P1”, “P2” and “P3” in Table 10 indicate sub-samples cut from each tile (Appendix D).

### 3.3.5- Moisture expansibility

The expansion of fired-clay materials is considered irreversible under natural environmental conditions. It starts as soon as the ceramic materials are removed from the kiln and occur throughout the years [23]. Ceramics moisture expansion is considered a time-dependent phenomenon where ceramic materials become more susceptible as they age. This phenomenon is believed to be largely dependent on the proportion of amorphous or vitreous phases present in the ceramic material [23].

The dilation resulting from water absorption is presented in Figure 7 and Table 11. In Appendix E the sub-samples used in the moisture expansibility tests are presented. After 60 h, the dilation had not stabilized yet, keeping a slow increasing pace. SP1-A2 showed the largest expansibility while SP1-A1 was the least water-expansive. The expansibility of SP1-A6 could not be measured for technical reasons.

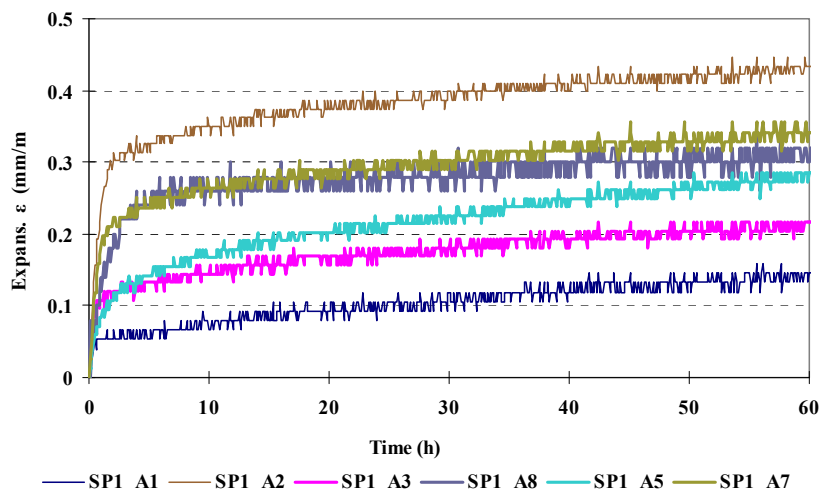


Figure 7 - Samples water dilation with time

Table 11 – Readings and values of water expansibility at 48 h

Samples	$l_0$ (mm)	$L_0$ (mm)	$L_f$ (mm)	$(L_f-L_0)$ (mm)	$\epsilon$ (mm/m)
<b>SP1-A1-P5</b>	75.66	2.486	2.496	0.01	<b>0.13</b>
<b>SP1-A2-P3</b>	82.86	2.836	2.871	0.035	<b>0.42</b>
<b>SP1-A3-P3</b>	83.10	2.215	2.232	0.017	<b>0.21</b>
<b>SP1-A5-P3</b>	84.12	2.328	2.35	0.022	<b>0.26</b>
<b>SP1-A6-P3</b>	69.59	nd	nd	nd	<b>nd</b>
<b>SP1-A7-P3</b>	76.00	2.005	2.03	0.025	<b>0.33</b>
<b>SP1-A8-P3</b>	50.00	2.450	2.465	0.015	<b>0.30</b>

In Table 11,  $l_0$  is the dry sample length;  $L_0$  the initial transducer reading,  $L_f$  the final transducer reading and  $\epsilon$  the moisture expansibility at 48 h.

### 3.3.6- Thermal expansibility

The thermal expansion of composite materials can be roughly considered as an additive property of all the crystalline and glass phases present in the material [24]. Azulejos being a layered material made up of a thin glaze layer, largely vitreous, and a larger ceramic layer with a high proportion of crystalline phases, their thermal expansibility bears the contribution of both layers with the ceramic body in principal prevailing. The sub-samples used in the thermal expansibility tests are presented in Appendix E and the results obtained shown in Figure 8 and Table 12.

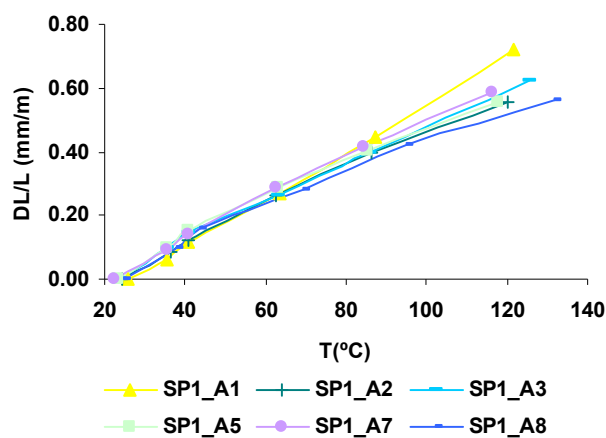


Figure 8 - Thermal expansion curves of the sample tiles.

Table 12 - Thermal expansibilities of the sample tiles.

Sample	Coeff. thermal exp. ( $\xi$ ) °C <sup>-1</sup>	R <sup>2</sup>	dL/L (mm/m) ( $\Delta T = 25^\circ\text{C}$ )
SP1-A1-P5	7.9E-03	0.999	0.20
SP1-A2-P3	6.9E-03	0.992	0.17
SP1-A3-P3	6.6E-03	0.999	0.16
SP1-A5-P3	6.8E-03	0.992	0.17
SP1-A6-P3	nd	nd	nd
SP1-A7-P3	7.1E-03	0.994	0.18
SP1-A8-P3	6.9E-03	0.990	0.17

In Table 12, the coefficient of thermal expansion was found by linear regression of the measurements and  $R^2$  is the correlation coefficient measuring the goodness of fit. The last column indicates the expansion expected for an increase of 25°C in the temperature of that tile.

As can be seen, the thermal expansibilities are largely similar with a temperature difference of about 25°C resulting in a thermal expansion of 0.024 to 0.030 mm in a 15cm square tile. Such expansions should, however, not be minimized since they add to the moisture expansions and in a panel several meters across can bring about large stresses, causing interference between the tiles with damage to their glaze and ultimately resulting in potential detachment from the walls.

#### 4- CONCLUSIONS

Several physical, chemical and mineralogical properties of a set of historical azulejos ranging from the 17<sup>th</sup> to the early 19<sup>th</sup> centuries have been measured or assessed. The results allowed a better understanding of the composition and behaviour of the samples and are indicative of the properties of historical Portuguese azulejos. The similarity of some of the results points to a similar use of raw materials and/or production techniques indicating the possibility of a common geographical origin (probably the Lisbon workshops). The results obtained allowed a better understanding of the correlations between the physical-chemical and mineralogical properties and the decay mechanisms and forms. Characterization of a larger and more representative number of samples would be necessary to encompass the particularities of the different provenances, types, and decay patterns of historic Portuguese azulejos. This work is planned to be done within a future research project and the results fed into a data base called LNEC-AZUL which has started to be built with the results now obtained. The database will have initially the form of an Excel file but can be easily upgraded to an Access database format when justified by its size. The purpose of the database is to consistently gather the analytical information obtained in order to be able to use this information in future azulejos studies. The database is organized by physical, chemical and mineralogical properties and it is hoped to feed it with results already obtained on previous studies, as well as results published by other researchers.

## **ACKNOWLEDGEMENTS**

Solange Muralha contributed to the XRF analyses that were performed under her supervision at Universidade Nova de Lisboa (UNL);

Susana Coentro of the Vicarte Institute of UNL helped with the quantification of the XRF results;

Luis Nunes performed the open porosity, hydric and thermal expansion measurements. João Junior did the MIP measurements;

Susana Couto performed the XRD and TGA-DTA measurements and analysis.

## **BIBLIOGRAPHIC REFERENCES**

- 
- <sup>1</sup> Sanjad, Thais A B C e Da Costa, Marcondes L, 2009, Azulejaria histórica em Belém do Pará: Contribuição tecnológica para réplicas e restauro, Edição do autor, Belém: UFPA/SEDECT.
  - <sup>2</sup> Antunes J L, 1992, Caracterização de azulejos do século XVII: Estudos para a sua consolidação, Tese de Mestrado em Engenharia Química, Instituto Superior Técnico.
  - <sup>3</sup> Coroado J and Gomes C, Physico-chemical characterization of ceramic glazed wall tiles dated of the 17th century, from the "Convento de Cristo", in Tomar, Portugal; Proceedings of the 7th European Meeting of Ancient Ceramics (EMAC'03). *Trabalhos de Arqueologia* 42, pp. 33 - 39.
  - <sup>4</sup> Carvalho A P, Vaz M F, Samora M J and Pires J, Characterisation of ceramic pastes of Portuguese ancient tiles, *Materials Science Forum*, 2006, Vol. 514-516, pp. 1648-1652.
  - <sup>5</sup> Perera M, Lacerda-Aroso T, Gomes M J M, Mata A, Alves L C and Colomban P, Ancient Portuguese ceramic wall tiles ("Azulejos"): Characterization of the glaze and ceramic pigments, *Journal of Nano Research*, 2009, 8, pp. 79-88.
  - <sup>6</sup> Coentro S X, Estudo da camada pictórica na azulejaria portuguesa do século XVII, Série Teses de Mestrado TM 30, LNEC, Lisboa 2011.

- 
- <sup>7</sup> Mimoso J-M, Santos Silva A, Abreu M, Costa D, Gonçalves Diaz T and Coentro S, Decay of historic azulejos in Portugal: an assessment of research needs, in Proc. Int.Sem.Conservation of Glazed Ceramic Tiles- research and practice, LNEC, Lisbon, April 2009.
- <sup>8</sup> Mimoso, J-M., "Levantamento em obra de patologias em azulejos históricos- visitas realizadas em 2009-2010", LNEC Research Report 22/2010 DM, Lisbon, January 2011
- <sup>9</sup> Mimoso J-M, Pereira S R M, Santos Silva A, A research on manufacturing defects and decay by glaze loss in historical Portuguese azulejos, LNEC Research Report 24/2010 DM, Lisbon, January 2011.
- <sup>10</sup> Matthes W E, Vidrados Cerámicos: Fundamentos, Propriedades, Recetas, Métodos, Ediciones Ómega, Barcelona.
- <sup>11</sup> Cultrone G, Rodrigues-Navarro C, Sebastian E, Cazalla O and de la Torre M J, Carbonate and silicate phase reactions during ceramic firing, Eur. J. Mineral, 2001, 13, pp. 621-634.
- <sup>12</sup> Amorós J L, Orts M J, Mestre S Garcia-Ten J and Feliu C, Porous single-fired wall tile bodies: Influence of quartz particle size on tile properties, Jour. Eur. Ceram. Soc., 2010, 30, pp. 17-28.
- <sup>13</sup> Coentro, S X, Mimoso, J-M and Silva, S S, Investigação da morfologia da interface vidrado/chacota em azulejos históricos, Relatório LNEC 27/2010-NPC, 2010.
- <sup>14</sup> Nunes, Luis, 2005, Uncertainty of tests and measurements in a testing laboratory of natural stones, LNEC, Relatório 313/05 NCMC, LNEC, 2005..
- <sup>15</sup> LERO PE-15, Ensaio de determinação da porometria por mercúrio, Manual de Procedimentos de Ensaio, LNEC, 1996.
- <sup>16</sup> E 412, 1993, Materiais em pó. Determinação da superfície específica. Método de B.E.T, Especificação LNEC.

- 
- <sup>17</sup> LERO PE-10, Ensaio de determinação do coeficiente de dilatação por absorção de água, Manual de Procedimentos de Ensaio, LNEC, 1996.
- <sup>18</sup> EN 14581, 2005, Natural stone test methods - Determination of linear thermal expansion coefficient.
- <sup>19</sup> Musthafa A M, Janaki K and Velraj G, Microscopy, porosimetry and chemical analysis to estimate the firing temperature of some archaeological pottery shreds from India, *Microchemical journal*, 2010, 95, pp.311-314.
- <sup>20</sup> Perés-Rodrigues J L, Maqueda C, Justo A, Morillo E and Jimenez de Haro M C, Characterization of decayed ceramic sculptures decorating the Pardon portico of Seville cathedral, Spain, *Applied Clay Sciences*, 9, 1994, pp. 211-223.
- <sup>21</sup> Sanjad T A B C, Angélica R S, Oliveira M M and Costa W A M, Caracterização mineralógica de azulejos de Salvador e Belém dos séculos XVI, XVII e XIX, *R. Esc. Minas Ouro Preto*, 2004, 57, 4, pp. 255-260.
- <sup>22</sup> Trindade M J, Dias M I, Coroado J and Rocha F, Mineralogical transformations of calcareous rich clays with firing: a comparative study between calcite and dolomite rich clays from Algarve, Portugal, *Applied Clay Science*, 2009, 42, pp. 345-335.
- <sup>23</sup> Segadães A M, Carvalho M A and Ferreira H C, Using phase diagrams to deal with moisture expansion, *Ceramics International*, 2003, 29, pp. 947-954.
- <sup>24</sup> Strnad Z, *Glass-Ceramic Materials: Glass Science and Technology* 8, Elsevier, 1986, pp. 174-175.

---

Lisboa, Janeiro de 2011

**VISTOS**

O Chefe do NPC



**João Manuel Mimoso**  
Investigador Coordenador

A Chefe do NMM



**Maria Manuela Salta**  
Investigadora Coordenadora

O Director do  
Departamento de Materiais



**Arlindo Freitas Gonçalves**  
Investigador Coordenador

**AUTORIA**



**Sílvia Morais Pereira**  
Doutorada em Eng<sup>a</sup> Química  
Estagiária do LNEC



**João Manuel Mimoso**  
Investigador Coordenador



**António Santos Silva**  
Investigador Auxiliar



## APPENDIX A – XRF SPECTRA AND REFERENCE SAMPLES USED FOR AZULEJOS GLAZE AND BISCUIT ANALYSIS

Bellow are presented exemplificative spectra of the XRF results for the ceramic biscuit (Figure 9) and glaze (Figure 10) respectively.

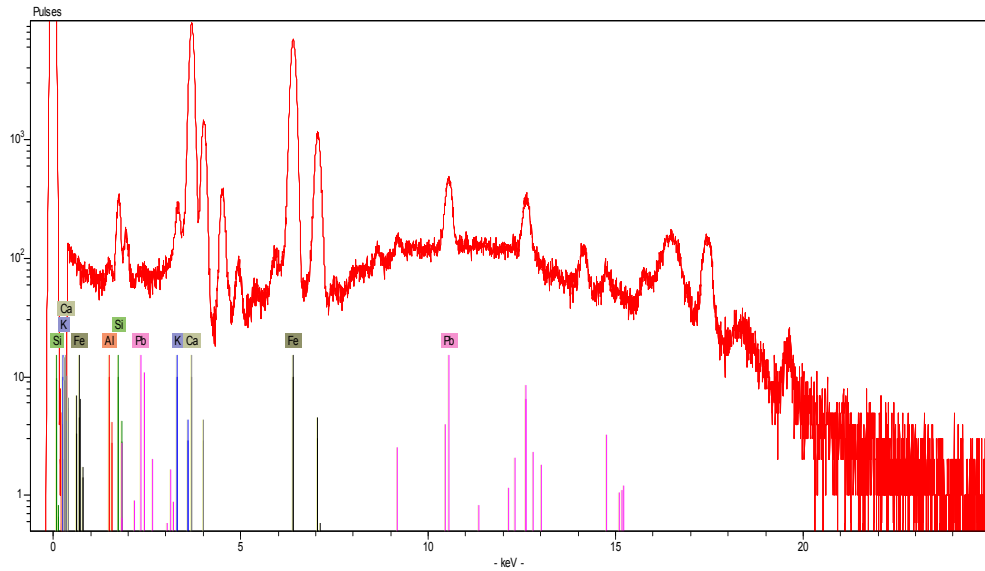


Figure 9 - XRF spectrum of SP1-A1 biscuit.

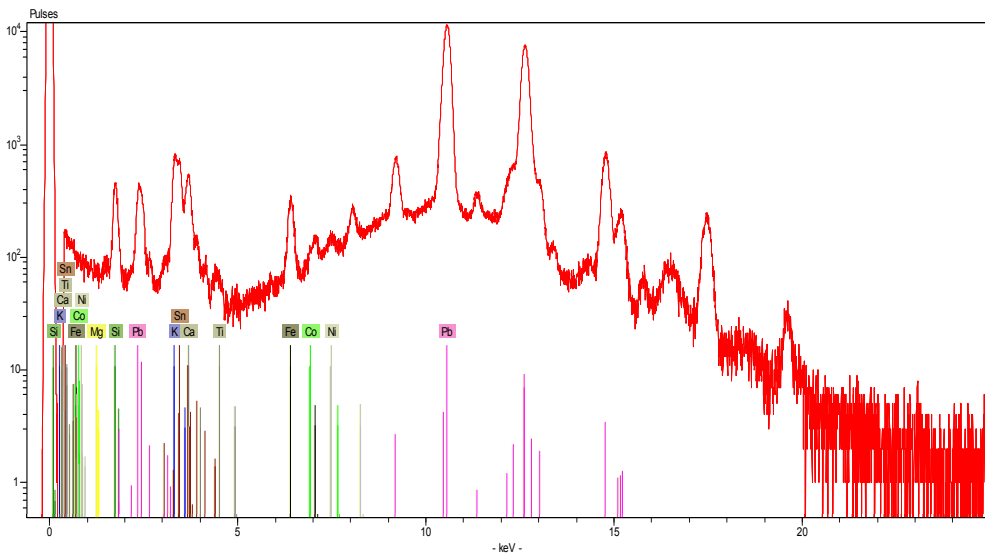


Figure 10 - XRF spectrum of SP1-A1 glaze.

The percent composition of the reference samples used for the XRF calibration is presented in Table 13 together with the expected accuracy for the quantitative elemental analyses.

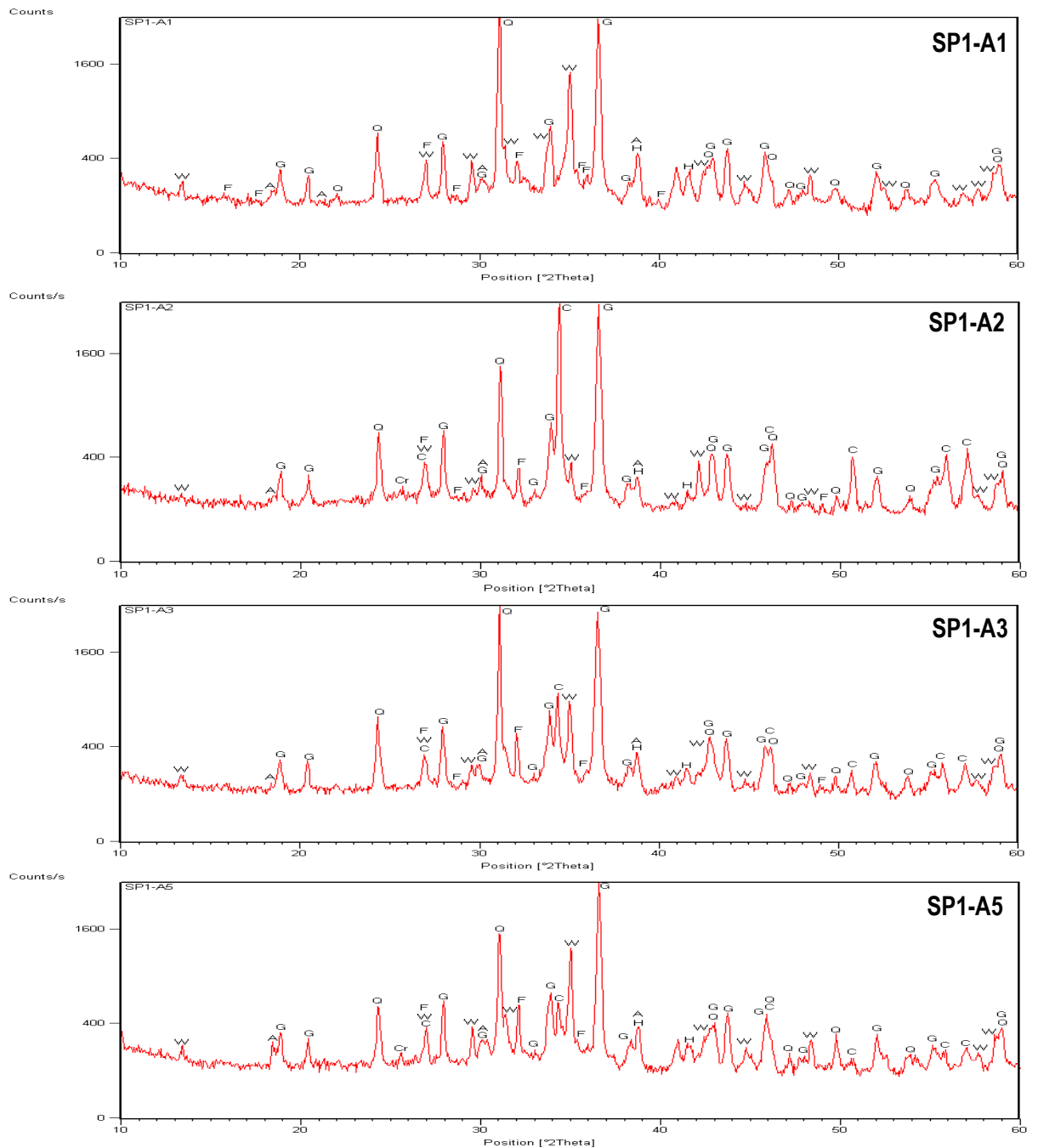
Table 13 - Standards used for Glaze and biscuit quantification and indicative accuracy measurements (%)

	<b>Red Brick Clay 679 (%)</b>	<b>Plastic Clay 98b (%)</b>	<b>CMOG C (%)</b>	<b>UN LeadTin (%)</b>	<b>Ceramics accuracy* (%)</b>	<b>Glaze accuracy* (%)</b>
<b>Al<sub>2</sub>O<sub>3</sub></b>	20.8	27.02	0.87	2.58	70	23
<b>BaO</b>	0.0482	-	11.4	-	2	
<b>CaO</b>	0.23	0.1	5.07	2.37	16	5
<b>Cr<sub>2</sub>O<sub>3</sub></b>	0.0159	0.017	0.18	-		22
<b>CuO</b>	-	-	1.13	-	2	
<b>Fe<sub>2</sub>O<sub>3</sub></b>	12.94	1.69	0.34	0.02	46	7
<b>K<sub>2</sub>O</b>	2.93	3.38	2.84	2.67	8	5
<b>Li<sub>2</sub>O</b>	0.0152	0.046	-	-		
<b>MgO</b>	1.25	0.59	2.76	-		
<b>MnO</b>	-	0.015	-	-		13
<b>Na<sub>2</sub>O</b>	0.18	0.2	1.07	3.22		
<b>P<sub>2</sub>O<sub>5</sub></b>	-	-	0.14	-	0	
<b>PbO</b>	-	-	36.7	44.3	9	
<b>Sb<sub>2</sub>O<sub>5</sub></b>	-	-	0.03	-	0	
<b>SiO<sub>2</sub></b>	52.07	57.01	36.15	40.8	7	10
<b>SnO<sub>2</sub></b>	-	-	0.19	4.02	74	
<b>SrO</b>	0.0086	0.022	0.29	-	2	33
<b>TiO<sub>2</sub></b>	0.96	1.35	0.79	-		21
<b>ZnO</b>	-	-	0.05	-	6	
<b>OH</b>	8.55	8.56	-	-		
<b>Total</b>	100%	100%	100%	100%		

\* (standard measured value – standard reference content)/standard reference content

## APPENDIX B – XRD DIFFRACTOGRAMS

In the next figure (Figure 11) are presented the diffractograms of the samples:





## APPENDIX C – TGA-DTA CURVES

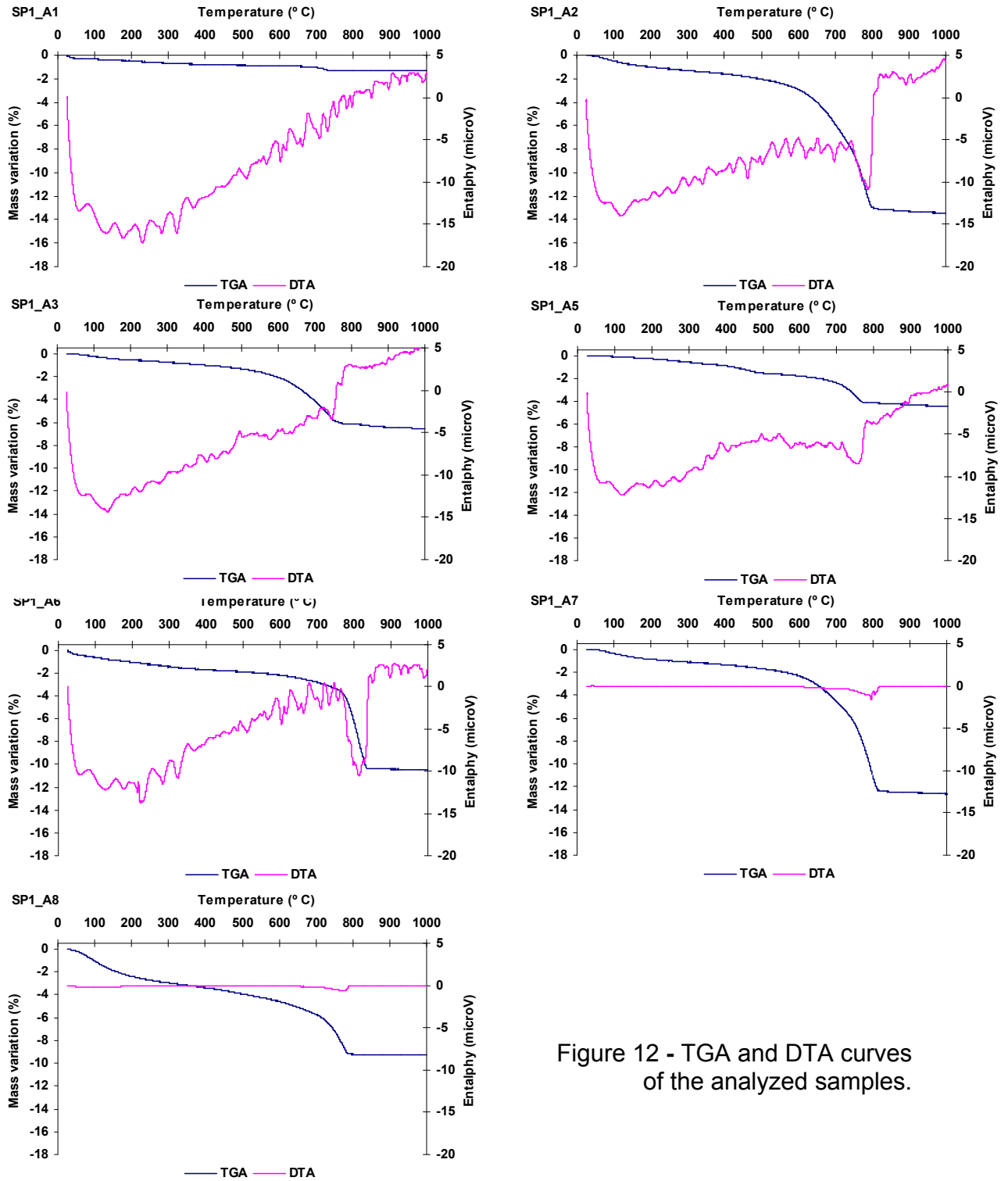


Figure 12 - TGA and DTA curves of the analyzed samples.

## APPENDIX D – SUB-SAMPLES USED FOR WATER IMBIBITIONS TESTS

The azulejo samples were cut in several pieces and those sub-samples marked with a “P” code and shown in Figure 13 were used for the water imbibition tests after isolating their lateral sides with an epoxy resin.

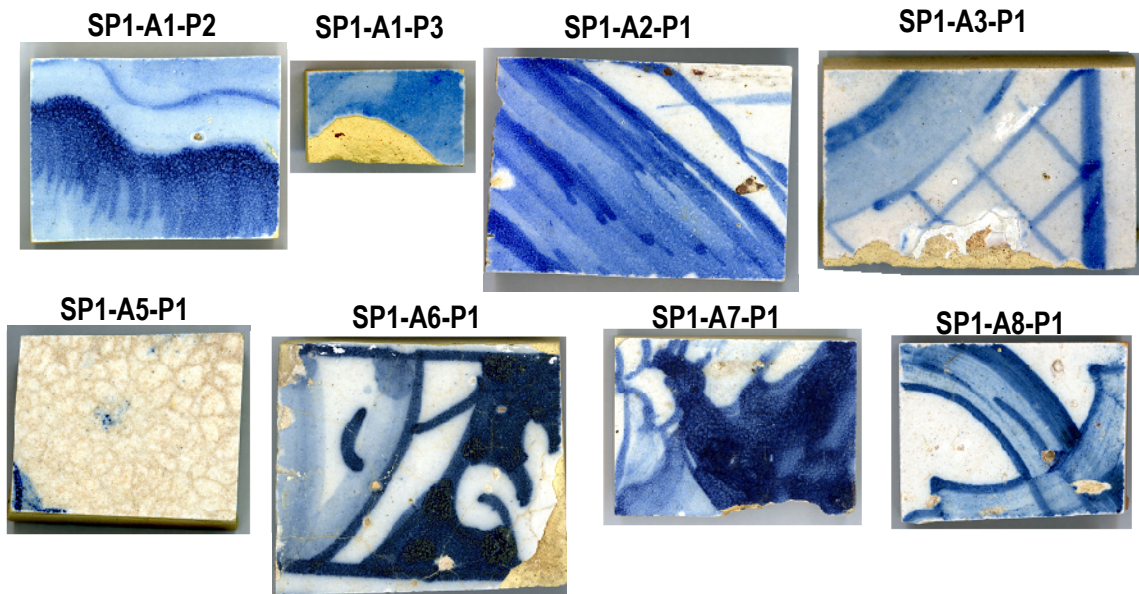
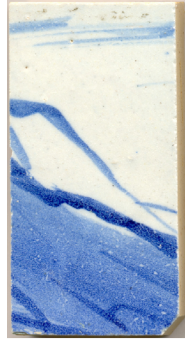


Figure 13 – Sub-samples from the azulejo tiles studied during water imbibition tests

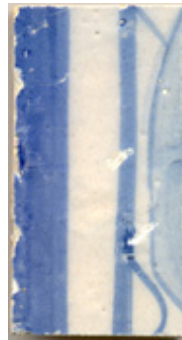
**APPENDIX E – SUB-SAMPLES USED FOR THE MOISTURE DILATION AND THERMAL EXPANSIBILITY TESTS**



**SP1-A1-P5**



**SP1-A2-P3**



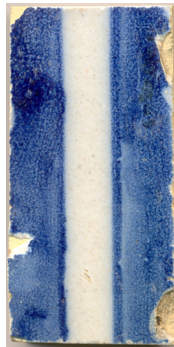
**SP1-A3-P3**



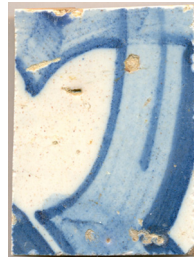
**SP1-A5-P3**



**SP1-A6-P3**



**SP1-A8-P3**



**SP1-A8-P3**

Figure 14 - Azulejo sub-samples used for the moisture and thermal expansion tests.

